Narrow Line Photoassociation in an Optical Lattice

T. Zelevinsky,[1] M. M. Boyd,[1] A. D. Ludlow,[1] T. Ido,[1,2] J. Ye,[1] R. Ciuryło,[3] P. Naidon,[4] and P. S. Julienne[4]

[1] *JILA, National Institute of Standards and Technology and University of Colorado, and the Department of Physics, University of Colorado, Boulder, CO 80309-0440, USA*
[2] *PRESTO, Japan Science and Technology Agency, 4-1-8 Honcho, Kawaguchi, 332-0012, Japan*
[3] *Instytut Fizyki, Uniwersytet Mikołaja Kopernika, ul. Grudziądzka 5/7, 87-100 Toruń, Poland*
[4] *Atomic Physics Division, National Institute of Standards and Technology, Gaithersburg, MD 20899-8423, USA*

(Dated: October 12, 2018)

With ultracold ^{88}Sr in a 1D magic wavelength optical lattice, we performed narrow line photoassociation spectroscopy near the $^1S_0$–$^3P_1$ intercombination transition. Nine least-bound vibrational molecular levels associated with the long-range 0_u and 1_u potential energy surfaces were measured and identified. A simple theoretical model accurately describes the level positions and treats the effects of the lattice confinement on the line shapes. The measured resonance strengths show that optical tuning of the ground state scattering length should be possible without significant atom loss.

PACS numbers: 34.80.Qb, 32.80-t, 32.80.Cy, 32.80.Pj

Photoassociation (PA) spectroscopy [1, 2] is a valuable tool for studies of atomic collisions and long-range molecules [3, 4, 5, 6, 7, 8, 9]. In contrast to conventional molecular spectroscopy that probes the most deeply bound vibrational levels of different electronic states, PA spectroscopy excites the vibrational levels close to the dissociation limit, where the molecular properties depend mostly on the long-range dipole-dipole interatomic interactions. Molecular potentials are much simpler at long range than at short range, and are directly related to the basic atomic properties such as the excited state lifetime and the s-wave scattering length.

In this Letter, we report the use of PA spectroscopy to resolve nine least-bound vibrational levels of the $^{88}Sr_2$ dimer near the $^1S_0$–$^3P_1$ intercombination line. Our identification of these levels is required for tuning of the ground state scattering length with low-loss optical Feshbach resonances [10]. This is of great interest for Sr, since magnetic Feshbach resonances are absent for the ground state, and the background scattering length is too small to allow evaporative cooling [9]. In contrast to prior PA work that utilizes strongly allowed transitions with typical line widths in the MHz range, here the spin-forbidden $^1S_0$–$^3P_1$ line has a natural width of 7.5 kHz. This narrow width allows us to measure the least-bound vibrational levels that would otherwise be obscured by a broad atomic line, and to observe characteristic thermal line shapes even at μK atom temperatures. It also permits examination of the unique crossover regime between the van der Waals and dipole-dipole interactions, that occurs in Sr near the $^1S_0$–$^3P_1$ dissociation limit. This access to the van der Waals interactions ensures large bound-bound Franck-Condon factors, and may lead to more efficient creation of cold ground state Sr_2 molecules with two-color PA than what is possible using broad transitions. Bosonic ^{88}Sr is ideal for narrow line PA because of its hyperfine-free structure and a high isotopic abundance (83%). In addition, Sr is a candidate atom for optical clocks [11, 12, 13], and PA spectroscopy could help determine density shifts for various clock transitions.

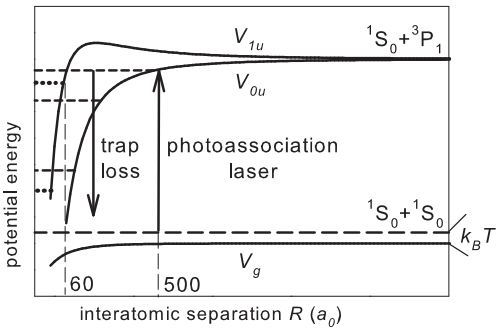

FIG. 1: Schematic diagram of the long-range Sr_2 molecular potentials (not to scale). The ground and excited molecular states coincide with two ground state atoms, and with one ground and one excited state atom, respectively, at large internuclear separations. The ground state has *gerade* symmetry and its energy is given by the potential V_g, while the excited state *ungerade* potentials that support dipole transitions to the ground state are V_{0u} and V_{1u}, the latter with a small repulsive barrier. All vibrational states of 0_u and 1_u (dashed and dotted lines, respectively) are separated by more than the natural line width, permitting high resolution PA spectroscopy very close to the dissociation limit when the atoms are sufficiently cold.

To enable long interrogation times needed for narrow line photoassociation, we trap Sr atoms in a 1D optical lattice. This technique also suppresses recoil shifts and Doppler broadening and thus simplifies the PA line shapes. The specially chosen lattice wavelength ($\lambda_{\rm magic}$) induces state-insensitive AC Stark shifts that minimize the perturbing effects of the lattice [14].

Figure 1 illustrates the relevant potential energy curves for the Sr_2 dimer as a function of interatomic separation R. The photoassociation laser at 689 nm induces allowed transitions between the separated $^1S_0$ atom continuum at a temperature T to the vibrational bound levels of the excited *ungerade* potentials V_{0u} and V_{1u}, corresponding

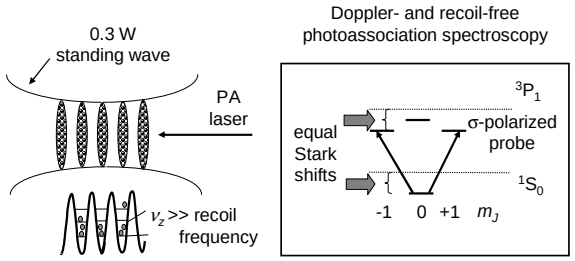

FIG. 2: Experimental configuration. The 2 μK atoms are confined in a 1D optical lattice in the Lamb-Dicke regime that allows Doppler- and recoil-free photoassociation spectroscopy. The lattice laser intensity is large enough to confine most atoms in the ground motional state. The 689 nm weak PA laser co-propagates with the lattice. The 914 nm lattice wavelength ensures that $^1S_0$ and the $m_J = \pm 1$ sublevels of $^3P_1$ are Stark-shifted by equal amounts.

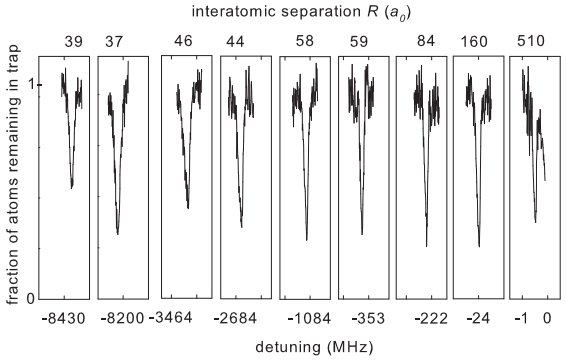

FIG. 3: The spectra of the long-range Sr_2 molecule near the $^1S_0 - ^3P_1$ dissociation limit. The horizontal scale is marked on the rightmost panel; different PA laser intensities were used for each spectrum due to largely varying line strengths. The top labels indicate the interatomic separations that correspond to the classical outer turning points of each resonance.

to the total atomic angular momentum projections onto the internuclear axis of 0 and 1, respectively. Although our calculations, based on the coupled channels method in Ref. [15], account for the Coriolis mixing between the 0_u and 1_u states, this mixing is small enough that 0_u and 1_u are good symmetry labels for classifying the states. Including the Coriolis mixing is necessary in order to fit the observed 0_u and 1_u bound state energies. Only s-waves (total ground state molecular angular momentum $J = 0$) contribute to the absorption (excited state $J = 1$) at our low collision energies. The long-range potentials are given by the C_6/R^6 van der Waals and C_3/R^3 dipole-dipole interactions, plus a rotational term $\propto 1/R^2$,

$$V_{0u} = -C_{6,0u}/R^6 - 2C_3/R^3 + h^2 A_{0u}/(8\pi^2 \mu R^2), \quad (1)$$
$$V_{1u} = -C_{6,1u}/R^6 + C_3/R^3 + h^2 A_{1u}/(8\pi^2 \mu R^2), \quad (2)$$

where h is the Planck constant, μ is the reduced mass, $A_{0u} = J(J+1) + 2$, and $A_{1u} = J(J+1)$. The values of C_3, $C_{6,0u}$, and $C_{6,1u}$ are adjusted in our theoretical model so that bound states exist at the experimentally determined resonance energies. Since our modeling of the PA energy levels due to long-range interactions is not sensitive to the details of short-range interactions, the latter are represented by simple 6-12 Lennard-Jones potentials whose depths are chosen to approximately match those in Ref. [16]. The coefficient C_3 can be expressed in terms of the atomic lifetime τ as $C_3 = 3\hbar c^3/(4\tau\omega^3)$, where $\hbar\omega$ is the atomic transition energy and c is the speed of light. Since the C_3 and C_6 interactions have comparable magnitudes in the region of R relevant to the energy levels we observe, the standard semiclassical analysis based on a single interaction $\propto R^{-n}$ [17] is not applicable.

The experiment is performed with ~ 2 μK ^{88}Sr atoms that are trapped and cooled in a two-stage magneto-optical trap (MOT) [18, 19]. As the atoms are cooled in the 689 nm narrow line $^1S_0 - ^3P_1$ MOT, they are loaded into a 1D far-detuned optical lattice [13], which is a 300 mW standing wave of 914 nm light with a 70 μm beam waist at the MOT. This results in 10^5 atoms with the average density of about $3 \times 10^{12}/\text{cm}^3$, after the MOT is switched off. The axial trapping frequency in the lattice is $\nu_z \sim 50$ kHz, much larger than the 5 kHz atom recoil frequency and the 7.5 kHz line width, resulting in Doppler- and recoil-free spectroscopy if the PA laser is collinear with the lattice beam. Figure 2 illustrates the lattice configuration. The polarizations of the lattice and PA lasers are linear and orthogonal in order to satisfy the λ_{magic} condition at 914 nm [14]. The choice of λ_{magic} ensures that $^1S_0$ and the magnetic sublevels of $^3P_1$ that are coupled to $^1S_0$ by the PA laser are Stark shifted by equal amounts, resulting in the zero net Stark shift for the transition and consequently eliminating inhomogeneous Stark broadening and shifts of the PA lines. A 689 nm diode laser used for PA is offset-locked to a cavity-stabilized master laser with a sub-kHz spectral width [11, 13].

To trace out the molecular spectra, the PA laser frequency is stepped, and after 320 ms of photoassociation at a fixed frequency the atoms are released from the lattice and illuminated with a 461 nm light pulse (resonant with $^1S_0 - ^1P_1$) for atom counting. At a PA resonance, the atom number drops as excited molecules form and subsequently decay to ground state molecules in high vibrational states or hot atoms that cannot remain trapped. Figure 3 shows the nine observed PA line spectra near the dissociation limit.

The line fits for the free-bound transitions are based on a convolution of a Lorentzian profile with a thermal distribution of initial kinetic energies [20], as schematically shown in Fig. 4 (a). In the 1D optical lattice, we work in the quasi-2D scattering regime, since $T \sim 2$ μK $\sim \nu_z/k_B$ (k_B is the Boltzmann constant), and the axial motion is quantized. For weak PA laser intensities used here, the total trap loss rate is a superposition of loss rates K_ε for

atoms with thermal energies $\varepsilon \equiv h^2k^2/(8\pi^2\mu)$,

$$K_\varepsilon(\nu) = \frac{h}{\mu}\frac{\gamma^2 l_{\rm opt}}{(\varepsilon/h+\nu-\nu_0)^2+(\gamma+\gamma_1)^2/4}, \qquad (3)$$

where ν and ν_0 are the laser and molecular resonance frequencies expressed as detunings from the atomic $^1S_0{-}^3P_1$ line, $\gamma \simeq 15$ kHz is the line width of the excited molecular state, $\gamma_1 \simeq 25$ kHz is a phenomenological parameter that accounts for the observed line broadening, $l_{\rm opt}$ is the optical length [10] discussed below, and only s-wave collisions are assumed to take place. While the total 3D PA loss rate is

$$K_{3D}(T,\nu) = \frac{2}{\sqrt{\pi}}\int_0^\infty K_\varepsilon(\nu)e^{-\varepsilon/k_BT}\frac{\sqrt{\varepsilon}d\varepsilon}{(k_BT)^{3/2}}, \qquad (4)$$

the 2D loss rate is

$$K_{2D}(T,\nu) = \int_0^\infty K_\varepsilon(\nu+\nu_z/2)e^{-\varepsilon/k_BT}\frac{d\varepsilon}{k_BT}. \qquad (5)$$

Dimensional effects appear in Eq. (5) as a larger density of states at small thermal energies (*i.e.* no $\sqrt{\varepsilon}$ factor), and as a red shift by the zero-point confinement frequency $\nu_z/2$. Another property of a 2D system (not observed here due to small probe intensities) is a lower bound on power broadening near $T \sim 0$, fixed by the zero-point momentum [21]. Equation (5) assumes only collisions in the motional ground state of the lattice potential. Although 50% of our atoms are in excited motional states, using a more complete expression yielded essentially the same line shapes. If any local atom density variations associated with PA are neglected and the temperature is assumed to be constant during probing, then the atom density evolution is given by

$$\dot{n} = -2Kn^2 - n/\tau_l, \qquad (6)$$

where $\tau_l \sim 1$ s is the lattice lifetime, from which we calculate the number of atoms remaining in the lattice.

The measured PA resonances ν_0 were reproduced theoretically by adjusting the C_3 and C_6 parameters as well as the short-range interatomic potentials. The measured and calculated ν_0 are compared in Table I. The positions

0_u Measured (MHz)	0_u Calculated (MHz)	1_u Measured (MHz)	1_u Calculated (MHz)
-0.435(37)	-0.418	-353.236(35)	-353.232
-23.932(33)	-23.927	-2683.722(32)	-2683.729
-222.161(35)	-222.152	-8200.163(39)	-8112.987
-1084.093(33)	-1084.091		
-3463.280(33)	-3463.296		
-8429.650(42)	-8420.124		

TABLE I: The comparison of measured and calculated molecular resonance frequencies, for both 0_u and 1_u potentials.

of the measured lines are found by fitting Eqs. (3-6) to the data (see Fig. 4). Both 2D and 3D line shape models were applied, without an appreciable difference in the obtained optical lengths. However, the 2D model yields ν_0 corrections of +15(10) kHz that are included in Table I. The measurement errors in the Table are a combination of a 30 kHz uncertainty of the atomic reference for the PA laser, and of the systematic and statistical reproducibility. The calculated ν_0 results are based on the coupled channels model [15] and were obtained using $C_3 = 0.007576$ au ($\tau = 21.35$ μs), $C_{6,0u} = 3550$ au, and $C_{6,1u} = 3814$ au (1 au is $E_h a_0^3$ for C_3 and $E_h a_0^6$ for C_6, where $E_h = 4.36\times10^{-18}$ J and $a_0 = 0.0529$ nm). However, the model limitations, such as insufficient knowledge of the short-range potentials, require the following uncertainties in the long-range parameters: $C_3 = 0.0076(1)$ au ($\tau = 21.4(2)$ μs), $C_{6,0u} = 3600(200)$ au, and $C_{6,1u} = 3800(200)$ au. The theoretical results for the two PA lines at detunings over 8 GHz disagree with experiment by 0.1-1% due to a high sensitivity to the short-range potentials, while all the other lines fit well within the specified uncertainties of as low as 10^{-5}.

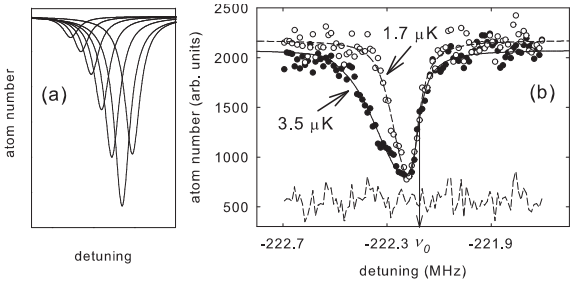

FIG. 4: (a) A line is schematically shown as a sum of Lorentzians with positions and amplitudes given by a continuous thermal distribution. (b) The measured line shapes of the −222 MHz transition at 1.7 μK (open circles) and 3.5 μK (filled circles), clearly showing the effect of temperature on the red side of the line. The bottom trace shows the residuals of the 1.7 μK curve fit.

Since the width of the Sr intercombination line is in the kHz range, even ultracold temperatures of a few μK contribute significant thermal broadening. Figure 4 (b) shows two spectra of the −222 MHz PA line taken at $T = 1.7$ μK and $T = 3.5$ μK (T was measured from the time-of-flight atom cloud expansion). The spectrum of the hotter sample manifests thermal broadening as a tail on the red-detuned side.

A photoassociation line depth is given by the optical length [10], $l_{\rm opt}$, a parameter proportional to the free-bound Franck-Condon factor and the PA laser intensity. It is useful for specifying the laser-induced changes in both elastic and inelastic collision rates that lead to optical control of the atomic scattering length and to atom loss, respectively. The optical lengths were obtained from the data and calculated from the Franck-Condon factors under the assumption of a zero ground state background

scattering length [9]. For the -0.4 MHz line, the experimental $l_{\rm opt}/I \simeq 4.5\times10^5\ a_0/({\rm W/cm^2})$, while the theoretical value is $9.0\times10^5\ a_0/({\rm W/cm^2})$, where I is the PA laser intensity. Significant experimental uncertainties may arise from the calibration of the atomic density and the focused PA laser intensity. In addition, we observe line broadening γ_1, most likely a result of the residual magnetic field, and any variation in this extra width can lead to $l_{\rm opt}$ error. The -0.4 MHz resonance is special due to its very large classical turning point, and its effective optical length increases with decreasing ε, while $l_{\rm opt}$ is energy-independent for the other lines (due to the Wigner threshold law [22]). Therefore, the reported effective $l_{\rm opt}$ values for the -0.4 MHz line are based on the 2 μK sample temperature with the 1 μK zero-point energy. In addition, the fitted $l_{\rm opt}$ for this resonance was multiplied by 2.5 to obtain the value quoted above, since our calculations show that 60% of the photoassociated and decayed atoms have insufficient kinetic energies to leave the ~ 10 μK deep trap. The measured and calculated $l_{\rm opt}$ for the other PA lines can differ by up to an order of magnitude, but both decrease rapidly as the magnitude of the detuning increases and are of the order of $l_{\rm opt}/I = 1\ a_0/({\rm W/cm^2})$ for the most deeply bound levels. The theoretical optical length of the -222 MHz line was found to have the largest dependence on the assumed ground state scattering length due to its sensitivity to the nodal structure of the ground state wave function.

Intercombination transitions of alkaline earths such as Sr are particularly good candidates for optical control of the ground state scattering length, $a_{\rm opt}$, because there is a possibility of large gains in $a_{\rm opt}$ with small atom losses. In fact, using the -0.4 MHz PA line with the measured $l_{\rm opt} \sim 5\times10^5\ a_0\ {\rm cm^2/W}$ will allow tuning the ground state scattering length by [10] $a_{\rm opt} = l_{\rm opt}(\gamma/\delta)f \simeq \pm300\ a_0$, where the PA laser with $I = 10\ {\rm W/cm^2}$ is far-detuned by $\delta = \pm160$ MHz from the molecular resonance, and the factor $f = (1+(\gamma/2\delta)^2(1+2kl_{\rm opt})^2)^{-1} \simeq 0.8$ accounts for the power broadening for 3 μK collisions. In contrast, optical tuning of the scattering length in alkali ^{87}Rb [23] achieved $a_{\rm opt} = \pm90\ a_0$ at much larger PA laser intensities of 500 W/cm^2. In addition, the Sr system at the given parameter values will have a loss rate of [10] $K = (2h/\mu)a_{\rm opt}\gamma/(2\delta) \simeq 2\times10^{-14}\ {\rm cm^3/s}$, while the loss rate in the ^{87}Rb experiment was $2\times10^{-10}\ {\rm cm^3/s}$. The overall optical length gain of over 5 orders of magnitude is possible for the Sr system because the narrow intercombination transition allows access to the least-bound molecular state, and the PA line strength increases with decreasing detuning from the atomic resonance (see Fig. 1 in Ref. [10]). The above $a_{\rm opt}$ and K values accessible with the -0.4 MHz resonance result in the elastic and inelastic collision rates of $\Gamma_{\rm el} \sim \sqrt{(2\varepsilon/\mu)}8\pi a_{\rm opt}^2 n \sim 600/{\rm s}$ and $\Gamma_{\rm inel} \sim 2Kn \sim 0.1/{\rm s}$, respectively. The favorable $\Gamma_{\rm el}/\Gamma_{\rm inel}$ ratio may enable evaporative cooling. A stringent constraint on the use of narrow-line optical Feshbach resonances is the proximity of the atomic transition. In the above example, the scattering rate of the PA laser photons due to the $^1{\rm S}_0{-}^3{\rm P}_1$ atomic line is $\Gamma_s \sim 40/{\rm s} \sim \Gamma_{\rm el}/15$. Excessive one-atom photon scattering can cause heating and loss of atoms from the lattice.

Another application of narrow line PA is potentially efficient production of cold molecules in the ground state. Our bound-bound Franck-Condon factor calculations show that over 50% of the molecules electronically excited to the -222 MHz level decay to the last ground state vibrational level (distributed between $J = 0, 2$).

In summary, we have measured a series of nine vibrational levels of the $^{88}{\rm Sr}_2$ dimer near the $^1{\rm S}_0{-}^3{\rm P}_1$ intercombination transition. The 20 μs long lifetime of $^3{\rm P}_1$, combined with the magic wavelength optical lattice technique, allowed direct probing of the least-bound state, and observation of thermal photoassociation line shapes even at ultracold μK temperatures, with explicit dimensional effects. We have characterized the strengths of the molecular resonances, and shown that the least-bound state should allow a unique combination of extensive, yet low-loss optical control of the ^{88}Sr ground state scattering length that may enable efficient evaporative cooling.

We thank N. Andersen for stimulating discussions, and acknowledge financial support from NIST, NRC, NSF, ONR, and the National Laboratory FAMO in Toruń.

[1] J. L. Bohn and P. S. Julienne, Phys. Rev. A **60**, 414 (1999).
[2] K. M. Jones *et al.*, Rev. Mod. Phys., in press.
[3] C. McKenzie *et al.*, Phys. Rev. Lett. **88**, 120403 (2002).
[4] J. Léonard *et al.*, Phys. Rev. Lett. **91**, 073203 (2003).
[5] C. Degenhardt *et al.*, Phys. Rev. A **67**, 043408 (2003).
[6] Y. Takasu *et al.*, Phys. Rev. Lett. **93**, 123202 (2004).
[7] S. B. Nagel *et al.*, Phys. Rev. Lett. **94**, 083004 (2005).
[8] M. Yasuda *et al.*, Phys. Rev. A **73**, 011403(R) (2006).
[9] P. G. Mickelson *et al.*, Phys. Rev. Lett. **95**, 223002 (2005).
[10] R. Ciuryło *et al.*, Phys. Rev. A **71**, 030701(R) (2005).
[11] T. Ido *et al.*, Phys. Rev. Lett. **94**, 153001 (2005).
[12] M. Takamoto *et al.*, Nature **435**, 321 (2005).
[13] A. D. Ludlow *et al.*, Phys. Rev. Lett. **96**, 033003 (2006).
[14] T. Ido and H. Katori, Phys. Rev. Lett. **91**, 053001 (2003).
[15] R. Ciuryło *et al.*, Phys. Rev. A **70**, 062710 (2004).
[16] E. Czuchaj *et al.*, Chem. Phys. Lett. **371**, 401 (2003).
[17] R. J. LeRoy and R. B. Bernstein, J. Chem. Phys. **52**, 3869 (1970).
[18] T. H. Loftus *et al.*, Phys. Rev. Lett. **93**, 073003 (2004).
[19] T. H. Loftus *et al.*, Phys. Rev. A **70**, 063413 (2004).
[20] K. M. Jones *et al.*, Phys. Rev. A **61**, 012501 (1999).
[21] D. S. Petrov and G. V. Shlyapnikov, Phys. Rev. A **64**, 012706 (2001).
[22] E. P. Wigner, Phys. Rev. **73**, 1002 (1948).
[23] M. Theis *et al.*, Phys. Rev. Lett. **93**, 123001 (2004).